Active Ras Triggers Death in Glioblastoma Cells through Hyperstimulation of Macropinocytosis

Jean H. Overmeyer, Aparna Kaul, Erin E. Johnson, and William A. Maltese

Department of Biochemistry and Cancer Biology, University of Toledo College of Medicine, Toledo, Ohio

Abstract

Expression of activated Ras in glioblastoma cells induces accumulation of large phase-lucent cytoplasmic vacuoles, followed by cell death. This was previously described as autophagic cell death. However, unlike autophagosomes, the Ras-induced vacuoles are not bounded by a double membrane and do not sequester organelles or cytoplasm. Moreover, they are not acidic and do not contain the autophagosomal membrane protein LC3-II. Here we show that the vacuoles are enlarged macropinosomes. They rapidly incorporate extracellular fluid-phase tracers but do not sequester transferrin or the endosomal protein EEA1. Ultimately, the cells expressing activated Ras detach from the substratum and rupture, coincident with the displacement of cytoplasm with huge macropinosome-derived vacuoles. These changes are accompanied by caspase activation, but the broad-spectrum caspase inhibitor carbobenzoxy-Val-Ala-Asp-fluoromethylketone does not prevent cell death. Moreover, the majority of degenerating cells do not exhibit chromatin condensation typical of apoptosis. These observations provide evidence for a necrosis-like form of cell death initiated by dysregulation of macropinocytosis, which we have dubbed ''methuosis.'' An activated form of the Rac1 GTPase induces a similar form of cell death, suggesting that Ras acts through Rac-dependent signaling pathways to hyperstimulate macropinocytosis in glioblastoma. Further study of these signaling pathways may lead to the identification of other chemical and physiologic triggers for this unusual form of cell death. (Mol Cancer Res 2008;6(6):965–77)

Received 9/13/07; revised 1/29/08; accepted 2/24/08.
Grant support: NIH grants R01 CA34569 and R01 CA115495 and the Charlotte Geyer Foundation.
The costs of publication of this article were defrayed in part by the payment of page charges. This article must therefore be hereby marked *advertisement* in accordance with 18 U.S.C. Section 1734 solely to indicate this fact.
Note: Supplementary data for this article are available at Molecular Cancer Research Online (http://mcr.aacrjournals.org/).
J.H. Overmeyer and A. Kaul contributed equally to this work.
Current address for E.E. Johnson: Department of Genetics and Complex Diseases, Harvard School of Public Health, 665 Huntington Avenue, Boston, MA 02115.
Requests for reprints: William A. Maltese, Department of Biochemistry and Cancer Biology, University of Toledo College of Medicine, Block Health Sciences Building, Mail Stop 1010, 3035 Arlington Avenue, Toledo, OH 43614. Phone: 419-383-4161; Fax: 419-383-6228. E-mail: william.maltese@utoledo.edu

doi:10.1158/1541-7786.MCR-07-2036

Introduction

Glioblastoma is one of the most aggressive human brain tumors (1, 2). Despite efforts to improve surgical, radiologic, and chemotherapeutic treatment strategies, the prognosis for patients with glioblastoma remains poor. A major problem is that residual cells remaining after surgical resection of the primary tumor rapidly acquire resistance to chemotherapeutic drugs (3). In addition, glioblastomas often harbor mutations in genes that regulate programmed cell death (e.g., *PTEN, RB*, and *p53*), rendering them resistant to conventional proapoptotic stimuli (4). These characteristics have stimulated interest in identifying alternative pathways for inducing cell death in glioblastoma.

Apoptosis is the best characterized form of programmed cell death. However, nonapoptotic forms of cell death are now recognized as playing significant roles during embryonic development, neurodegeneration, and cancer regression (5). In these cases, loss of cell viability may occur in a manner that is independent of caspase activation. Autophagic cell death (type II programmed cell death) is the most widely studied form of nonapoptotic cell death. Its diagnostic morphologic feature is accumulation of autophagosomes and degradative autolysosomes (6). Autophagic death has been reported to occur in several types of cancer cells (7), but it has received particular attention in glioblastoma, where it can be induced by alkylating agents (8), arsenic trioxide (9), ionizing radiation (10), and rapamycin (11). Nevertheless, it remains controversial whether increased autophagic activity is actually a direct cause of cell death. Recent evidence supports the alternative view that accumulation of autophagosomes may signify a survival response intended to rid cells of misfolded proteins or damaged organelles (12-14).

In 1999, Chi et al. (15) reported that ectopic expression of activated Ras GTPase, which normally serves to stimulate cell proliferation, can trigger nonapoptotic cell death in glioblastoma and gastric carcinoma. This was described as autophagic death because the cells developed numerous cytoplasmic vacuoles. However, there have been no follow-up studies to confirm that the vacuoles induced by Ras are autophagosomes. In the present study, we have determined that the large vacuoles that accumulate in glioblastoma cells expressing activated H-Ras are in fact derived from macropinosomes. Cell rupture coincides with continued expansion of these macropinocytotic vacuoles. These findings provide evidence for a novel form of cell death characterized by hyperstimulation of vesicular fluid uptake and accumulation of swollen macropinosomes. We have termed this process methuosis (from the Greek word *methuo*, which means to drink to intoxication).

Results

Effects of Ectopic Expression of Activated Ras in Human Glioblastoma Cells

U251 cells harbor mutations in the proapoptotic genes *PTEN* and *p53* and are widely used as a model for human glioblastoma (16). To begin a detailed characterization of the cellular phenotype triggered by expression of activated Ras in glioblastoma cells, we generated a stable U251 glioblastoma cell line (U251-C18) that exhibits tightly controlled conditional expression of myc-tagged H-Ras(G12V) in response to the addition of doxycycline (Dox; Fig. 1A). Our initial observations of these cells generally agreed with those reported by Chi et al. (15). That is, coincident with expression of myc-tagged Ras(G12V), the cells became filled with lucent cytoplasmic vacuoles that are readily detected by phase-contrast microscopy (Fig. 1A). By day 6, there was a decrease in the number of viable cells in the cultures expressing H-Ras(G12V) compared with the controls (Fig. 1B). This coincided with the noticeable cell rounding and detachment from the dish, with abundant floating debris suggestive of cellular disintegration. In cultures harvested on day 6 after addition of Dox, detached cells accounted for ~10% of the total cell population (data not shown). Nearly 50% of these detached cells were nonviable when tested in a live/dead assay that measures the hydrolysis of calcein acetoxy methylester (live) and uptake of ethidium homodimer III (dead; Fig. 1C). On the other hand, the attached cells in the cultures expressing active Ras scored positive for viability (Fig. 1C) and exhibited DNA histograms with S-phase populations similar to the control cells growing without Dox (Supplementary Fig. S1). Although they were extensively vacuolated, the attached cells collected on day 6 after addition of Dox showed no significant decline in ATP levels compared with the cells maintained without Dox (Fig. 1D). However, consistent with their reduced viability, the detached cells exhibited a marked reduction in ATP concentration (Fig. 1D). Taken together, these findings imply that metabolic failure leading to cell death occurs abruptly at a late stage coincident with or after the detachment of the vacuolated cells. The long-term consequences of H-Ras(G12V) expression for cell survival are evident in colony-forming assays where addition of Dox resulted in an 85% to 90% reduction in the number of colonies (Fig. 1E).

The same pattern of vacuolization and cell degeneration was observed when Ras(G12V) was introduced into U251 cells by retroviral infection (Supplementary Fig. S2) or by transient nucleofection (17). Seven additional independently derived human glioma cell lines, some without mutations in *PTEN* (LN229) or *p53* (U87MG and A172; ref. 16), also exhibited a similar phenotype after expression of H-Ras(G12V) (Supplementary Fig. S2A). However, introduction of myc-H-Ras(G12V) into other commonly used cells (HeLa, HEp2, and HEK293) did not cause vacuolization (Supplementary Fig. S2B). As previously reported, the inactive GDP-locked (15, 17) or nonfarnesylated (17) forms of Ras did not cause vacuolization, indicating that the cellular phenotype is directly related to the activation of specific Ras signaling pathways.

Ras-Induced Vacuoles Are Distinct from Autophagosomes

Electron microscopy of glioblastoma cells expressing H-Ras(G12V) revealed numerous electron-lucent vacuoles ranging from 0.5 to 2 μm in diameter, with some larger vacuoles reaching 7 to 8 μm (Fig. 2A). The vacuoles were generally devoid of cytoplasmic components or organelles, although some contained unidentified membranous inclusions or small quantities of amorphous electron-dense material (Fig. 2A). At high magnification, the thickness of the membranes surrounding the vacuoles was estimated at 6 to 8 nm (Supplementary Fig. S3), consistent with a single membrane. The large electron-lucent vacuoles were clearly distinct from smaller structures fitting the description of "classic" autophagosomes (18), which have double membranes surrounding luminal cytoplasmic contents (Fig. 2A, *black arrows*).

To further confirm that the Ras-induced vacuoles were not derived from autophagosomes, we carried out immunofluorescence staining of the cells with an antibody against a well-established autophagosome marker, microtubule-associated protein light chain 3 (LC3). LC3 exists in a cytosolic form (LC3-I) and in a form that is conjugated to phosphatidylethanolamine on autophagosome membranes (LC3-II; ref. 19). The relative amount of LC3-II correlates with the number of autophagosomes induced by starvation and other stimuli (19). The LC3 antibody (Abgent, Inc.) reacts predominantly with LC3-II on Western blots. Therefore, we used this antibody to determine if LC3-II was localized to the vacuole membranes. As we have previously reported (17), myc-H-Ras(G12V) was localized in membranes surrounding the vacuoles (Fig. 2B). In contrast, LC3-II was detected in much smaller punctate structures (Fig. 2B). Confocal microscopy clearly showed that the large vacuoles circumscribed by myc-H-Ras(G12V) were separate from the LC3-II–positive autophagosomes (Fig. 2C).

Because the preceding study was done with cells that were transiently nucleofected, we were able to compare the cells expressing myc-H-Ras(G12V) with the adjacent nontransfected cells (Fig. 2B, *asterisks*). We noticed that the punctate LC3 fluorescence was more intense in the transfected cells, suggesting that autophagosomes might accumulate separately from the phase-lucent vacuoles. To explore this possibility, we determined the relative amount of LC3-II in stable U251-C18 cells with or without the expression of myc-H-Ras(G12V). As shown in Fig. 2D (*left*), expression of myc-H-Ras(G12V) was associated with a 2.7-fold increase in the amount of LC3-II, normalized to lactate dehydrogenase. However, this could reflect either an increase in autophagosome biogenesis (stimulation of cellular macroautophagy pathways) or a decreased lysosomal turnover of LC3-II. An established method that can be used to distinguish between these possibilities is to compare the levels of LC3-II in the presence and absence of lysosomal protease inhibitors (20). As shown in Fig. 2D (*right*), addition of protease inhibitors to uninduced cells (−Dox) caused a 3.2-fold increase in the basal level of LC3-II, consistent with the expected impairment of lysosomal LC3-II turnover. However, when myc-Ras(G12V) was induced by addition of Dox, there was an additional 2-fold increase in LC3-II above the level caused by addition of protease inhibitors alone. This indicates that much of the increase in LC3-II induced by expression of Ras(G12V) is related to an increase in autophagosome formation rather than a block in LC3-II turnover. Similar results were obtained when the cells were treated with

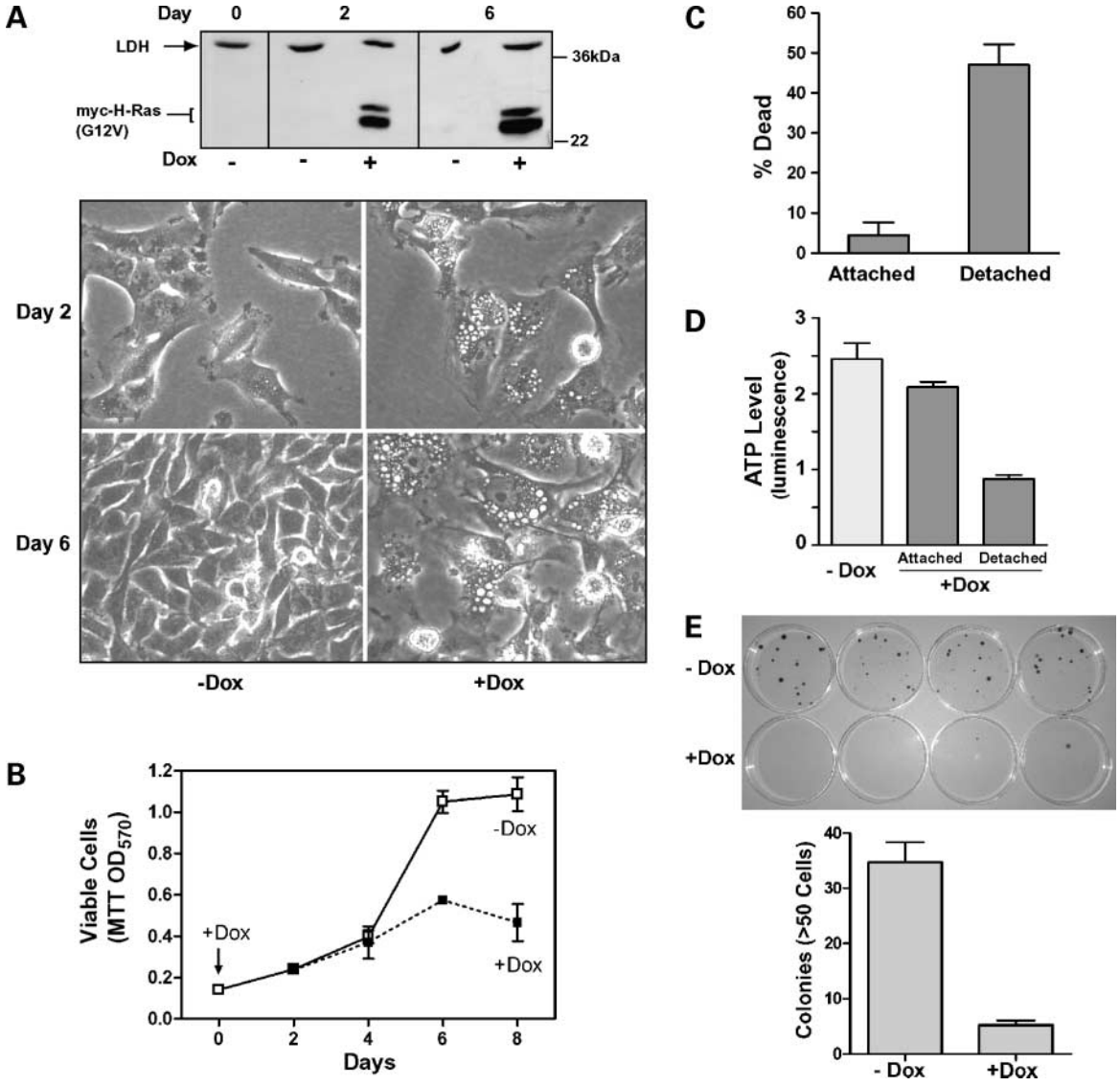

FIGURE 1. Expression of activated H-Ras induces cytoplasmic vacuolization and death of U251 glioblastoma cells. **A.** On day 0 (24 h after plating), U251-C18 glioblastoma cells were switched to medium containing 1 μg/mL Dox (*+Dox*) or maintained in medium without Dox (*−Dox*). Western blots show the expression of myc-tagged H-Ras(G12V) in parallel cultures at intervals after addition of Dox. Phase-contrast microscopy of the same cultures shows extensive accumulation of cytoplasmic vacuoles in the cultures expressing Ras(G12V). **B.** MTT assays show a decline in the number of viable cells in cultures expressing H-Ras(G12V). Points, mean determined from four separate cultures in a 96-well plate initially seeded at 5,000 cells per well; bars, SD. MTT was added directly to the medium to avoid losing detached cells. **C.** Live versus dead fluorescence assays were done on detached cells collected in the medium from three parallel cultures between day 4 and day 7 after addition of Dox. The attached cells from the same cultures were collected on day 7. For each determination, 50 cells were scored. **D.** ATP assays were done on attached or detached cells after 6 d in medium with or without Dox. Columns, mean determined from three separate cultures; bars, SD. **E.** Cells were plated for colony-forming assays as described in Materials and Methods. Twenty-four hours after plating, cultures were switched to medium with or without Dox. After 3 wk, colonies with >50 cells were counted. Columns, mean from four plates; bars, SD.

rapamycin, an inhibitor of mammalian target of rapamycin and a well-established inducer of macroautophagy (data not shown; ref. 21).

As shown in Fig. 3, expression of Ras(G12V) has identical effects on cell morphology and viability when expressed in a stable U251 cell line that we previously established as being resistant to proautophagic stimuli because of a knockdown of the autophagy protein, beclin-1 (22). This suggests that the increased autophagic activity detected in Fig. 2 is not required for the death of glioblastoma cells expressing activated Ras(G12V), and that cellular degeneration is most likely related to the progressive accumulation of the nonautophagic phase-lucent vacuoles.

Ras-Induced Vacuoles Are Enlarged Macropinosomes

In considering the possible origins of the phase-lucent vacuoles, we noted a previous study in which activated Ras was shown to stimulate macropinocytosis in fibroblasts (23). Macropinocytosis is a process whereby cells internalize extracellular fluid trapped beneath the projections of the plasma membrane termed ruffles or lamellipodia (24). Macropinosomes typically appear as phase-lucent vesicles ranging in

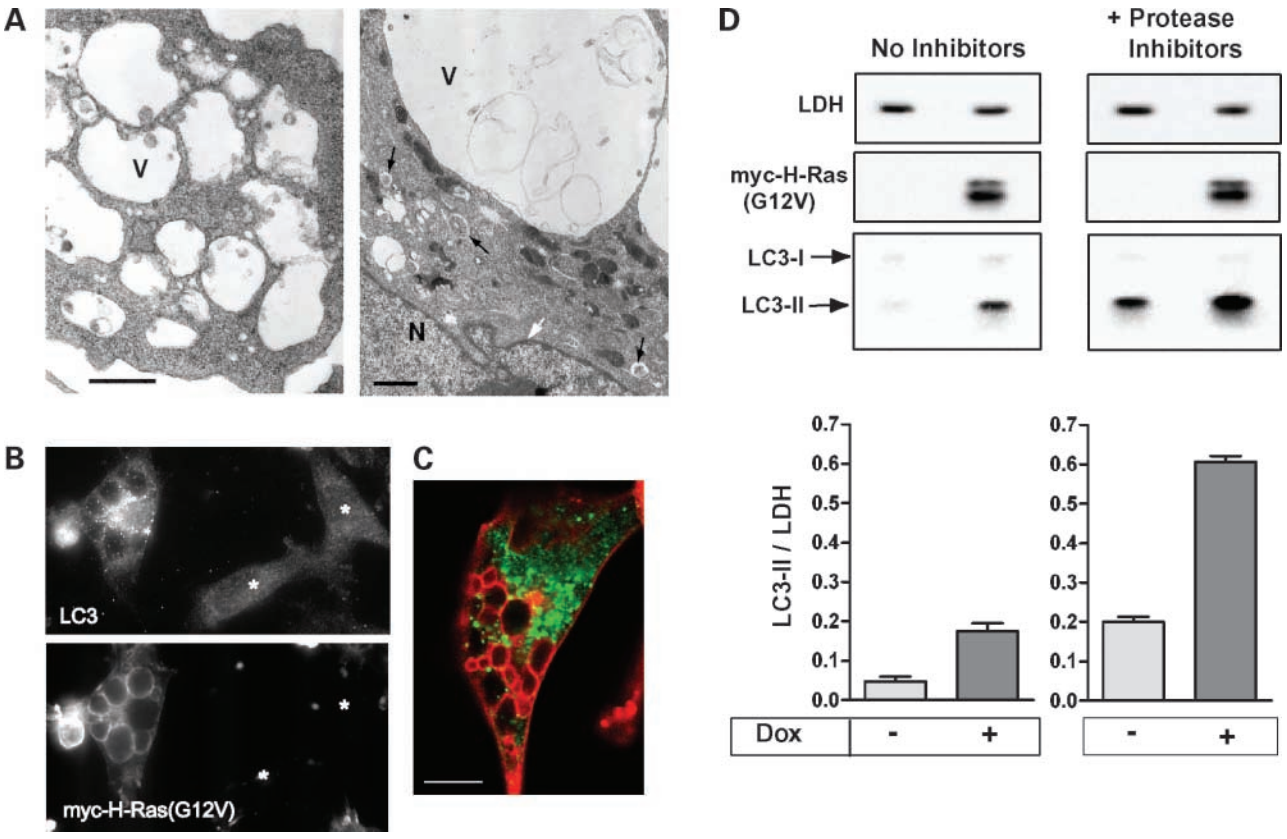

FIGURE 2. Vacuoles induced by activated Ras are distinct from autophagosomes. **A.** U251 cells were infected with myc-H-Ras(G12V) retrovirus to induce vacuoles and then examined by electron microscopy after 2 d. Vacuoles (*V*) are electron lucent and much larger than the typical autophagosomes with double-membrane morphology (indicated with *black arrows*). White arrow, nuclear membrane; N, nucleus. Bar, 1 μm. **B.** Nucleofected U251 cells transiently expressing myc-H-Ras(G12V) were costained with antibodies recognizing endogenous LC3 (*top*) and the myc epitope (*bottom*). Asterisks, cells in the same field that did not express myc-tagged Ras. **C.** A confocal image of stable U251-C18 cells incubated with Dox for 4 d, showing distinct localization of myc-H-Ras(G12V) (*red*) and endogenous LC3 (*green*; bar, 10 μm). **D.** Accumulation of the autophagosome marker LC3-II in cells expressing Ras(G12V). On the day after plating, U251-C18 cells were changed to medium with or without Dox as indicated. At the same time, the cultures received E64D and pepstatin A (*Protease Inhibitors*) or DMSO (*No Inhibitors*). After 2 d, immunoblot analysis was done to determine the levels of myc-Ras(G12V), lactate dehydrogenase (*LDH*), and LC3-II as described in Materials and Methods. Top, representative blots (scans from the Alpha Innotech imaging system) documenting expression of myc-H-Ras(G12V), LC3-II, and lactate dehydrogenase. Bottom, results obtained when the ratio of LC3-II to lactate dehydrogenase was quantified in triplicate samples.

diameter from 0.5 to 5 μm. Rapid incorporation of extracellular fluid-phase tracers is a hallmark of macropinosomes. When we added Lucifer yellow to the medium, cells expressing H-Ras(G12V) incorporated the tracer into many of the phase lucent vacuoles within 10 minutes (Fig. 4A). Quantification of Lucifer yellow internalization by flow cytometry showed a 3-fold increase in the uptake of the tracer into the +Dox cells expressing Ras(G12V), compared with the basal level of Lucifer yellow uptake in the −Dox controls (Fig. 4B). Preincubation with cytochalasin D, which disrupts the actin cytoskeleton involved in the formation of lamellipodia, had no effect on Lucifer yellow uptake in the −Dox cells, suggesting that most of the Lucifer yellow uptake in these cells is due to the basal activity of the endocytic pathway. In contrast, addition of cytochalasin D caused a 50% reduction of Lucifer yellow incorporation in +Dox cells after subtraction of the basal uptake attributed to endocytosis (Fig. 4B, *−Dox, +CytoD*).

Electron micrographs revealed numerous lamellipodia closing around regions of extracellular fluid to form nascent macropinosomes in the cells expressing H-Ras(G12V) (Fig. 4C). Control cells that were not expressing Ras also contained some lamellipodia, but closure of these structures to form enlarged macropinosomes was not evident (data not shown).

In addition to labeling macropinosomes, fluid-phase tracers can enter early endosomes. Macropinosomes lack a clathrin coat and can be distinguished from endosomes by their comparative inability to concentrate receptors (25). Therefore, to confirm that the vacuoles were derived from macropinosomes, cells expressing Ras(G12V) were subjected to short-term incubation with a bulk fluid-phase tracer, dextran-Alexa Fluor 488, together with a ligand for the transferrin receptor, transferrin-Alexa Fluor 594. The larger vesicles containing fluorescent dextran were distinct from the much smaller endosomes that sequestered transferrin (Fig. 4D). In accord with this finding, we observed that the phase-lucent vacuoles were separate from smaller punctate structures detected by immunofluorescence with an antibody against the well-known early endosomal protein EEA1 (Fig. 4E). These findings, coupled with the morphologic evidence in Fig. 4C, support the identification of the Ras-induced vacuoles as macropinosomes.

The lucent vacuoles induced by activated Ras are morphologically distinct from lysosomes and autolysosomes, which typically contain electron-dense organelle remnants or degraded cytoplasmic components (ref. 26; Figs. 2A and 4C). However, on the basis of morphology alone, it was difficult to rule out the possibility that some of the Ras-induced vacuoles might be swollen late endosomes, similar to those observed in cells where morphogenesis of multivesicular endosomes is disrupted by the inhibition of the class III phosphatidylinositol 3-kinase Vps34 (27, 28). Because the latter retained the acidic characteristic of late endosomes, they readily incorporated lysosomotropic agents (27). Therefore, to test the possibility that some of the Ras-induced vacuoles might be late endosomal compartments, we carried out supravital staining with Lysotracker Red. As shown in Fig. 5A, there was no clear overlap between the phase-lucent vacuoles and the compartments labeled with Lysotracker Red. Similar results were obtained when the cells were stained with acridine orange, which is sequestered in late endosomes, lysosomes, and autolysosomes (data not shown; refs. 29, 30). Additionally, there was no substantial overlap between the phase-lucent vacuoles and the compartments labeled with Magic Red RR, a cell-permeable peptide substrate that fluoresces when cleaved by cathepsin B (Fig. 5B). Taken together, these results support the conclusion that the majority of the phase-lucent vacuoles are derived from macropinosomes rather than late endosomes or lysosomes.

Although the vacuoles did not stain with markers for acidic or cathepsin-positive compartments (Fig. 5A and B), we found that many of them contained LAMP1, a membrane protein typically associated with lysosomes and late endosomes (Fig. 5C). Two possible models could explain this: In the first model, macropinosomes may fuse with late endosomes or lysosomes, acquiring LAMP1 and simultaneously neutralizing the interior of these compartments so that they cannot be

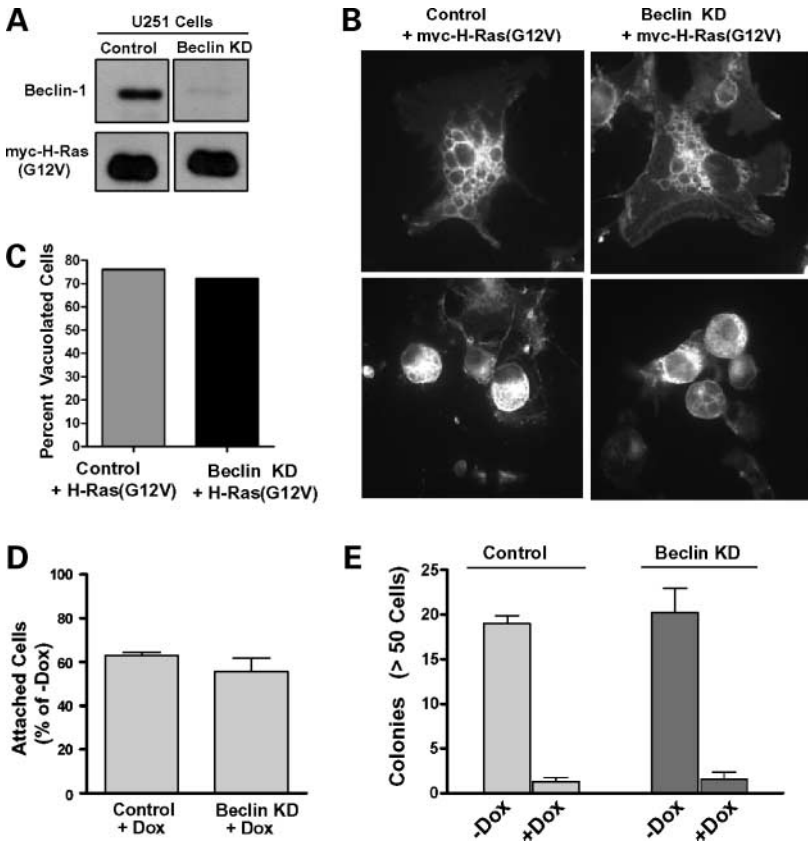

FIGURE 3. Suppression of the expression of the proautophagy protein beclin-1 does not interfere with Ras-induced vacuolation and cell death. **A.** U251 cells expressing nonspecific (*Control*) or beclin-specific RNAi (*Beclin KD*) were generated as described (16). These cells were nucleofected with the pCMV5*myc-H-Ras(G12V)* expression vector or empty vector and examined 24 h later. **A.** Western blots show that myc-Ras(G12V) was expressed equally in control and beclin KD cells. Expression of beclin-1 was reduced by >90%. Equal amounts of protein were loaded in each lane. **B.** Representative cells showing the immunofluorescence localization of myc-H-Ras(G12V) to prominent cytoplasmic vacuoles in control and beclin KD cells. Cell rounding and detachment occurred in both control and beclin KD cells. **C.** Percentage of vacuolated cells in the control and beclin KD cultures depicted in **B**. The values were determined by counting 100 cells in random photomicrographs using a threshold of two or more vacuoles (>0.5 μm diameter) per cell for a positive score. **D.** The stable tet-inducible U251-C18 cell line was infected with lentivirus containing inverted repeat stem-loop RNAi sequences matching a unique region of the human *beclin* mRNA or a "control" sequence that did not match any known GenBank entry. Beclin knockdown was verified to be >90% in beclin KD cells compared with controls. The control and beclin KD cell lines were then incubated with or without Dox as described in the legend to Fig. 1. On the 6th day after addition of Dox, the number of attached cells in control and beclin KD cultures expressing H-Ras(G12V) (+Dox) was determined and the results were expressed as the percent of the number of attached cells in parallel cultures without Dox. Columns, mean of separate determinations from three cultures; bars, SD. **E.** Aliquots of cells from the U251-C18 control and beclin KD cell lines were plated for colony-forming assays with or without addition of Dox to induce Ras(G12V) expression. The number of colonies was counted in three cultures from each group.

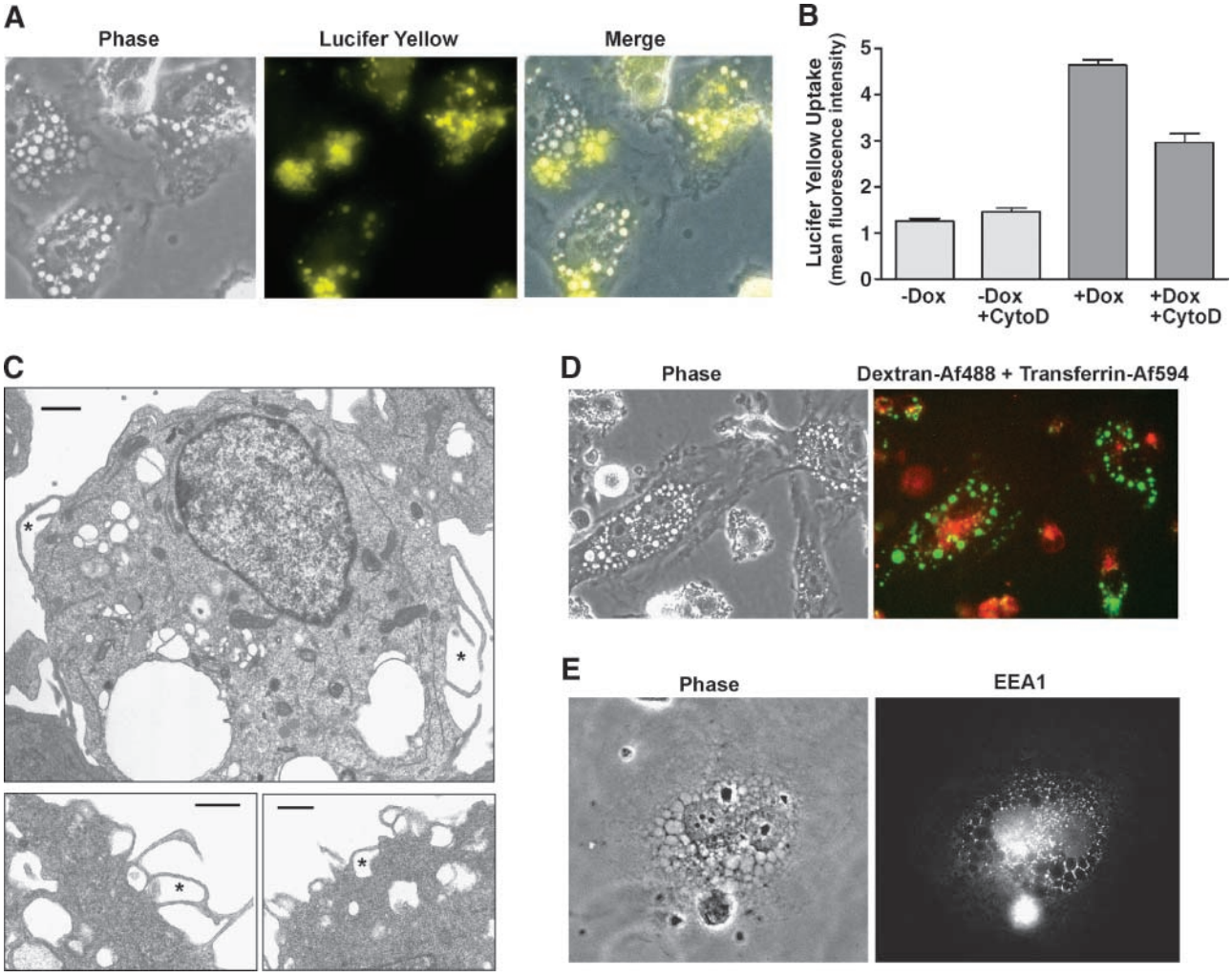

FIGURE 4. Vacuoles induced by Ras(G12V) in U251 cells exhibit characteristics of macropinosomes. **A.** Phase-lucent vacuoles incorporate the extracellular fluid-phase tracer Lucifer yellow. Live cells were incubated with Lucifer yellow for 15 min on the 4th day after they were induced to express myc-H-Ras(G12V) by the addition of Dox. **B.** U251-C18 cells maintained for 2 d with or without Dox were incubated with Lucifer yellow for 15 min and uptake of the tracer was quantified by flow cytometry. Where indicated, the cells were preincubated for 30 min with cytochalasin D (*CytoD*) before adding Lucifer yellow. **C.** Electron microscopy of attached U251-C18 cells expressing myc-H-Ras(G12V) reveals the presence of numerous lamellipodia that close to form nascent macropinosomes (*asterisks*). Bar, 1 μm. **D.** Vacuoles that incorporate the fluid-phase tracer dextran-Alexa Fluor 488 are separate from compartments that incorporate transferrin-Alexa Fluor 594. Live vacuolated cells were incubated with the indicated fluorescent probes for 15 min on the 4th day after induction of myc-H-Ras(G12V) with Dox. The same field of cells is shown in the phase-contrast and fluorescence micrographs. **E.** Vacuolated cells expressing myc-H-Ras(G12V) were fixed and subjected to immunofluorescence microscopy to localize the endosomal marker EEA1.

detected with acidophilic agents or cathepsin substrates. An alternative model is suggested by reports that LAMP1 can traffic directly to nonlysosomal compartments like early endosomes (31) or nascent phagosomes (32). Thus, the macropinosomes may remain separate from lysosomes while recruiting LAMP1 directly to their membranes. To discriminate between these models, we prelabeled the lysosomal compartments of vacuolated glioblastoma cells by incubating them with Lysotracker Red for 3 hours. Then, after removing the Lysotracker from the medium, we added fluorescent dextran for 4 hours to determine if the dextran-labeled compartments would merge with the prelabeled lysosomes (Fig. 5D). After 4 hours, we detected merger of some of the smaller dextran-labeled structures with the Lysotracker-positive compartments, presumably representing the fusion of endosomes with lysosomes. However, even after this extended period, the larger dextran-labeled vacuoles seemed to remain separate from the prelabeled lysosomal compartments (Fig. 5D). Similar results were observed when the cathepsin substrate Magic Red RR was used to prelabel the lysosomes (data not shown). These observations are consistent with the concept of direct recruitment of LAMP1 to the membranes of macropinocytotic vacuoles, with minimal fusion between these compartments and lysosomes.

Activated Rac1 Induces Cytopathology Similar to That Caused by Activated Ras

The mechanisms underlying macropinocytosis are poorly understood, but previous studies have implicated the Rac1 GTPase and its effector, PAK1, as key regulators of this process (33, 34). Because downstream targets of Ras include guanine

nucleotide exchange factors that can stimulate activation of Rac1 (e.g., Tiam1; ref. 35), we hypothesized that Rac1 might be positioned downstream from Ras in the pathway that triggers macropinosome accumulation in glioblastoma cells.

To test this possibility, we asked if expression of a constitutively active form of Rac1 could mimic the effects of Ras(G12V) in U251 glioblastoma cells. As shown in Fig. 6A and B, conditional expression of activated myc-Rac1(G12V) in U251 cells triggered a vacuolar phenotype closely resembling that observed with Ras(G12V). As in the case of cells expressing Ras(G12V), the viability of the cells expressing Rac1(G12V) declined between the 4th and 8th days after addition of Dox, coincident with extreme vacuolation and cell detachment (Fig. 6C). Moreover, the cells expressing Rac1(G12V) exhibited a substantial increase in the uptake of Lucifer yellow into the vacuolar structures (Fig. 6D). We have

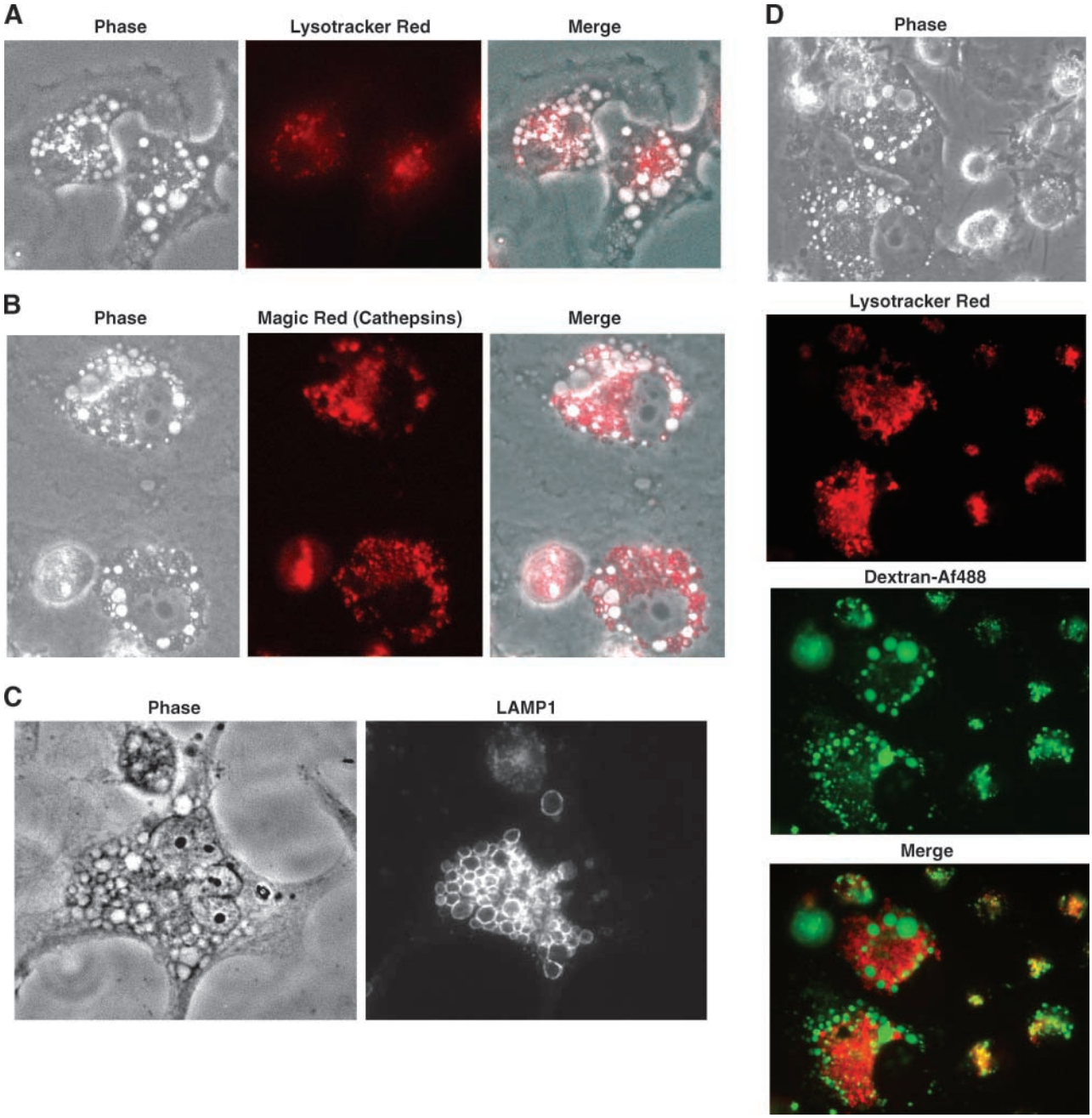

FIGURE 5. Vacuoles induced by Ras(G12V) in U251 cells are distinct from late endosomes and lysosomes. Four days after inducing U251-C18 cells to express myc-H-Ras(G12V), live cells were incubated with Lysotracker Red to label acidic compartments (**A**) or incubated with Magic Red-RR to label compartments containing cathepsin B activity (**B**). **C.** Vacuolated cells expressing Ras(G12V) were fixed and subjected to immunofluorescence microscopy to localize LAMP1. **D.** Vacuolated cells expressing Ras(G12V) were preincubated with Lysotracker Red (*red*) for 3 h, washed, and then incubated for 4 h with dextran-Alexa Fluor 488 (*green*). The phase-contrast image (*Phase*) at the top shows the same field of cells depicted in the fluorescent images.

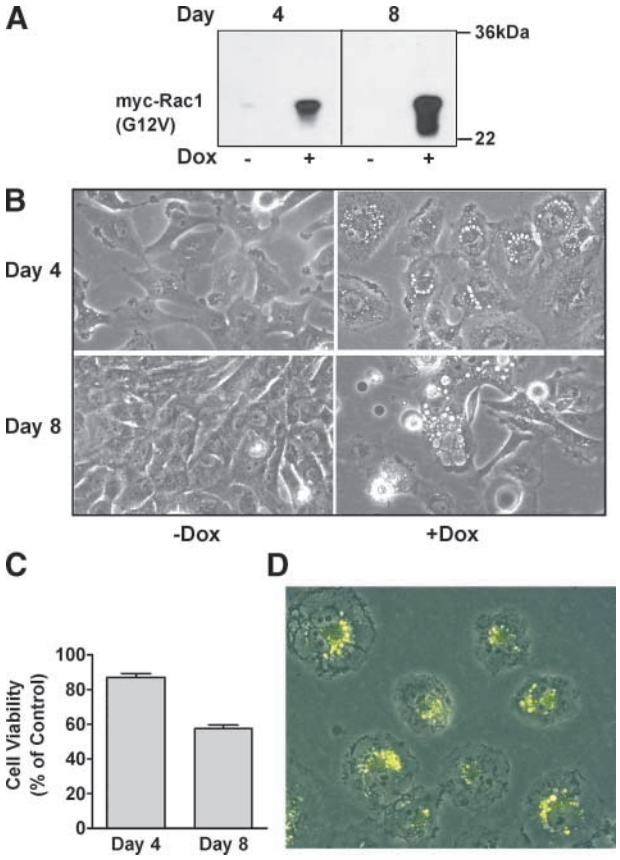

FIGURE 6. Activated Rac1 mimics the effects of activated Ras in glioblastoma cells. A stable U251 cell line for conditional expression of myc-Rac1(G12V) was generated as described in Materials and Methods. **A.** On day 4 and day 8 after addition of Dox, the expression of myc-Rac1(G12V) was checked by immunoblot analysis with an antibody against the myc epitope. **B.** Phase-contrast microscopy of the same cultures shows extensive accumulation of cytoplasmic vacuoles and cell detachment in the cultures expressing Rac1(G12V). **C.** MTT assays show a decline in the number of viable cells in the +Dox cultures compared with the −Dox controls. Columns, mean determined from six separate cultures in a 96-well plate; bars, SD. **D.** U251 cells expressing Rac1(G12V) incorporate Lucifer yellow into the phase-lucent vacuoles. Cells were incubated with Lucifer yellow for 15 min on the 4th day after addition of Dox. The micrograph shows a merge of the phase-contrast and fluorescence images of the live cells.

previously reported that the activated forms of other Rho-family GTPases (e.g., Cdc42 and RhoA) do not cause vacuolation of U251 cells (17). Thus, the hyperstimulation of macropinocytosis seems to be a specific effect of Ras(G12V) and Rac1(G12V).

The Mechanism of Cell Death in Glioblastoma Cells Expressing Activated Ras Is Distinct from Apoptosis

In their initial report describing the Ras-induced death of glioblastoma cells, Chi et al. (15) found no evidence for caspase activation in the vacuolated cells. However, in light of our observation that loss of cell viability coincides with detachment from the substratum (Fig. 1C), we reexamined this question by evaluating the cleavage of caspase substrates in both the attached and detached cell populations. As shown in Fig. 7A, there was no cleavage of poly(ADP-ribose) polymerase (PARP) or lamin A/C in the attached, mostly viable, vacuolated cells. However, in the detached cells, fragments of PARP and lamin A/C were detected at molecular weights consistent with caspase-3 cleavage. The sizes of these fragments were identical to those observed in cells treated with staurosporine, a known inducer of apoptosis (Fig. 7A). Examination of the portion of the PARP blot below 75 kDa did not reveal any 50-kDa fragments indicative of degradation by lysosomal proteases (36). In accord with the PARP cleavage, 49.6% of the detached cells stained positive for caspase-3 activity (Supplementary Fig. S4A), mirroring the percentage of nonviable cells in the detached population (Fig. 1C). Agarose gel electrophoresis revealed no evidence of DNA fragmentation in the attached cells, but the DNA recovered from the detached cells was extensively degraded, with detectable laddering suggestive of nucleosomal DNA fragmentation (Supplementary Fig. S4B).

To determine if the death of the cells expressing Ras(G12V) was dependent on caspase activation, we added the broad-spectrum caspase inhibitor carbobenzoxy-Val-Ala-Asp-fluoromethylketone (z-VAD-fmk) during the critical period (days 4-6) when loss of cell viability begins to occur. The PARP blots in Fig. 7B indicate that z-VAD-fmk was highly effective in blocking caspase activation. However, this did not prevent vacuolization (not shown) or loss of cell viability (Fig. 7C). Thus, although activation of caspases occurs in conjunction with the demise of glioblastoma cells, this is not an obligatory feature of the death mechanism. In separate studies, we also tested the ability of cathepsin and calpain inhibitors to preserve the viability of the vacuolated cells (Supplementary Fig. S5). Consistent with the absence of alternative 50-kDa PARP cleavage products, the lysosomal protease inhibitors were ineffective in preventing cell death induced by expression of Ras(G12V).

In light of the foregoing observations, we examined the morphology of the detached glioblastoma cells to determine if these cells exhibit typical features of apoptosis (Fig. 7D). Electron microscopy revealed that at least 80% of the detached cells contained numerous large cytoplasmic vacuoles with morphology similar to the macropinosomes described earlier in the attached cells (Figs. 2A and 4C). The cells were generally swollen to 20- to 30-μm diameter, compared with the attached cells, which typically ranged from 10 to 15 μm. In about half of the cell population, the expansion of vacuoles was so extreme that these structures filled most of the cytoplasmic space (Fig. 7D). Whereas some cells contained numerous vacuoles of various sizes (Fig. 7D, *i*), others contained only a few very large vacuoles (*ii* and *iii*), suggestive of an end-stage coalescence of these structures. In addition to the distorted cells with intact peripheral membranes, there were numerous remnants of cells that had ruptured (Fig. 7D, *iv*). However, even in the severely vacuolated or ruptured cells, the nuclei were generally intact and contained diffuse chromatin and a prominent nonfragmented nucleolus. These observations indicate that the morphologic features of the dying glioblastoma cells resemble the necrosis-like forms of cell death rather than classic apoptosis.

Discussion

The resistance of many types of cancer cells to apoptosis has stimulated interest in identifying nonapoptotic cell death

pathways that might be targeted to slow tumor progression. A number of distinct nonapoptotic forms of cell death have now been characterized. These include type II or autophagic cell death (5, 7, 12), paraptosis (37, 38), oncosis (39-41), and necroptosis (42, 43). Even the term necrosis, previously used to indicate "passive" cell death or the postmortem state of cells (39), has more recently been used to describe forms of programmed cell death that involve progressive lysosomal damage, leakage of lysosomal proteases, and early disruption of the cell membrane (44-47). In the present study, we provide a detailed characterization of a novel form of nonapoptotic cell death observed in glioblastoma cells on constitutive stimulation of Ras signaling pathways. The hallmark cytopathologic feature of this form of cell death is the marked accumulation of large fluid-filled vacuoles derived from macropinosomes. Electron microscopy shows a correlation between cellular disintegration and a progressive increase in the number and size of the macropinocytotic vacuoles. These observations are highly suggestive of a causal relationship between the dysregulation of macropinocytotic fluid uptake and the eventual metabolic collapse and rupture of the cells. Final proof of this interrelationship must await the development of new approaches for long-term inhibition of macropinocytosis because the drugs currently used to block this process (e.g., amiloride and cytochalasins) are toxic when applied to cultured cells for more than a few hours (48).

In contrast with an earlier report (15), we discovered that by examining detached cells expressing Ras(G12V), we could in fact detect caspase activation and DNA fragmentation. However, similar to the situation in most other forms of nonapoptotic death, caspase activation does not seem to be an obligatory step in the Ras-induced death program. Furthermore, our studies of cellular morphology did not show the typical cell shrinkage, blebbing, and nuclear chromatin condensation observed in apoptotic cells. Therefore, our results support the classification of Ras-induced macropinocytotic cell death as nonapoptotic. As discussed below, comparison with other known types of nonapoptotic death suggests that macropinocytotic cellular degeneration represents a unique form of cell death.

Autophagic death is now the most widely recognized type of nonapoptotic cell death. The diagnostic feature of this form of death is the proliferation of autophagosomes and autolysosomes that engulf cytoplasm and organelles and cannibalize the cell

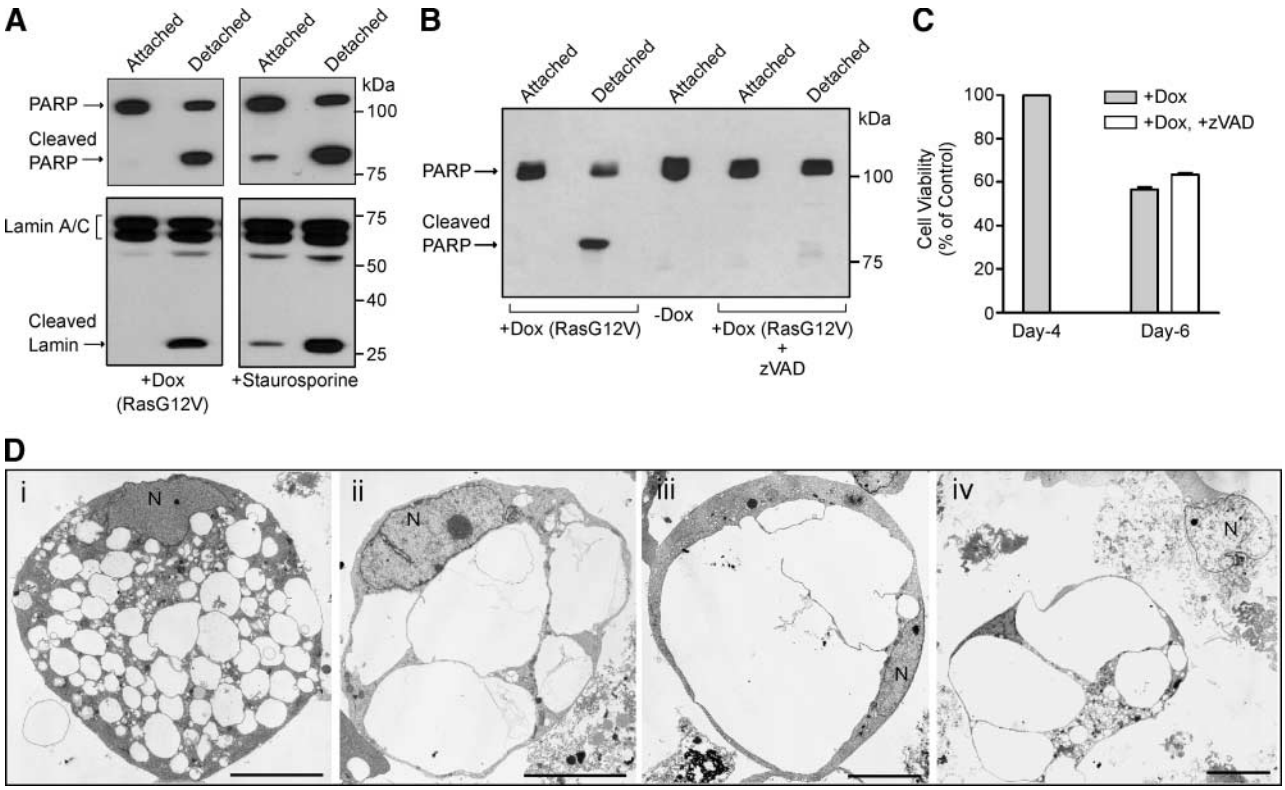

FIGURE 7. Progressive degeneration of glioblastoma cells expressing activated Ras involves macropinosome expansion and nonessential activation of caspases. **A.** Expression of myc-H-Ras(G12V) was induced by incubating stable U251-C18 cells with Dox. The medium was replaced every 2 d. Detached cells were collected between days 4 and 7. Attached cells were collected on day 7. As a positive control for apoptotic cleavage of PARP and lamin A/C, cells maintained without Dox were treated with staurosporine for 24 h. Immunoblots showing PARP (*top*) and lamin A/C (*bottom*) reveal cleavage products indicative of caspase activation. **B.** U251-C18 cells were seeded and maintained with or without Dox as described in Fig. 1. Starting on day 4, half of the +Dox cultures were changed to medium with 50 μmol/L z-VAD-fmk in DMSO. The −Dox cultures (no Ras expression) received DMSO alone. On day 6, the attached and detached cells were harvested for immunoblot analysis of PARP. **C.** MTT assays were done on day 4 and day 6, comparing the viability of the cells in the +Dox cultures with that of −Dox controls. Columns, mean of assays done on four wells of a 96-well plate; bars, SD. **D.** Electron micrographs of representative detached U251-C18 cells collected between days 4 and 6 after induction of Ras(G12V) expression. Bar, 10 μm.

(5, 12). In cells expressing activated Ras, the large macropinocytotic vacuoles that eventually fill the degenerating cells are morphologically distinct from autophagosomes. Although autophagosomes seem to accumulate in parallel with the macropinocytotic vacuoles, our studies with beclin-1 knockdown cells suggest that macropinocytotic vacuolization and cell death induced by Ras(G12V) can occur independent of the autophagy machinery. Thus, in this case, autophagy may reflect the attempt of the cells to survive under the adverse metabolic conditions created by rampant macropinosome accumulation rather than being a direct cause of cell death. This would be consistent with accumulating evidence that autophagy can function as a protective strategy against apoptosis or necrosis in cells subjected to metabolic stress (14).

The cytopathology induced by activated Ras or Rac is also distinct from several lesser-known forms of cell death. Necroptosis can be triggered by the stimulation of death receptors under conditions where caspases are inhibited (42, 43). Cell swelling and membrane rupture occur, but a massive increase in vesicular fluid uptake is not a diagnostic feature of necroptosis. Moreover, we have observed that necrostatin, a potent inhibitor of necroptosis, does not impede Ras-induced vacuolization or cell death.[1] Oncosis is a form of caspase-independent death typically caused by ischemia or disruption of ion pumps (41, 49). As in the case of the Ras-induced cell death, oncosis can include cell swelling, vacuolization, and membrane rupture. Cytoplasmic vacuolization also occurs in another distinctive form of cell death termed paraptosis (37). However, in both oncosis and paraptosis, the vacuoles are derived mainly from distended endoplasmic reticulum and/or mitochondria rather than macropinosomes. Finally, although cytoplasmic vacuolization is sometimes mentioned as a feature in various forms of necrosis-like cell death involving lysosomal damage, we have not detected alternative 50-kDa PARP cleavage products that would signal the leakage of lysosomal cathepsins associated with this form of necrosis (36), nor have we observed any mitigation of Ras-induced cell degeneration by treating glioblastoma cells with cathepsin or calpain inhibitors. In light of these differences from other types of cell death, and the unique association of cellular degeneration with hyperstimulation of macropinocytosis (cell drinking), we propose that this form of cell death be named "methuosis" (from the Greek word *methuo*, which means to drink to intoxication). Table 1 summarizes the features of methuosis in comparison with other reported forms of cell death.

Activating mutations in Ras have long been regarded as oncogenic because they result in chronic stimulation of signaling pathways important for cell proliferation (50). Activated Ras may also contribute to tumor progression by protecting transformed cells from apoptosis, although some reports have described opposite proapoptotic functions for Ras (51). The stimulation of a nonapoptotic death mechanism by activation of Ras highlights a relatively unexplored aspect of Ras signaling pathways. Our finding that activated Ras can induce vacuolization and cellular degeneration in a variety of human glioma cell lines, including those that harbor *PTEN* and *p53* mutations that render them relatively resistant to apoptosis (e.g., U251 and T98G), suggests that the presence of Ras-responsive pathways capable of hyperstimulating macropinocytosis and/or inhibiting the clearance or recycling of macropinosomes may be a general feature of human glioblastoma. If so, further delineation of the relevant signaling mechanisms could suggest ways to manipulate this pathway to trigger cell death in these intractable tumors. In this regard, our previous studies have indicated that stimulation of vacuolization in glioblastoma cells does not depend on conventional Ras effectors such as Raf, phosphatidylinositol 3-kinase, and Ral-GDS (17). In considering alternative possibilities, it is noteworthy that the Rac1 GTPase has been implicated as a regulator of macropinocytosis (33). Indeed, as we have shown here, expression of activated Rac1(G12V) in glioblastoma cells can mimic the effects of Ras(G12V). Because downstream targets of Ras include guanine nucleotide exchange factors like Tiam1, which can stimulate activation of Rac1 (35), our working hypothesis is that these exchange factors may be the key Ras effectors involved in transmitting signals via Rac to the macropinocytotic machinery.

Our studies, by comparing glioblastoma cells to HeLa, HEK293, and HEp2 cells, suggest that there is definite cell type specificity in the ability of Ras to stimulate methuosis. Similar conclusions were drawn by Chi et al. (15), who observed Ras-induced vacuolization in glioblastoma and two gastric cancer cell lines, but not in bladder carcinoma cells. Thus, obtaining a better understanding of the basis for the particular sensitivity of certain cell types to methuosis will be important for evaluating the therapeutic potential of this form of cell death. Our results with dextran tracers (Fig. 5D) indicate that, unlike normal macropinosomes, the Ras-induced vacuoles do not dissipate or fuse with lysosomal compartments after they are internalized. This raises the possibility that the explanation for the differential sensitivity to methuosis could reside not only at the level of induction of macropinocytosis but also at the level of intracellular trafficking or membrane channel function.

Another important question for future study is whether stimuli other than ectopic expression of Ras or Rac can provoke methuosis. In this regard, it is worth noting that cytoplasmic vacuolization is often mentioned as a morphologic feature of necrotic cell death caused by cytotoxic drugs or adverse environmental conditions, but there is seldom any indication about the specific origin of the vacuoles. Thus, it is conceivable that dysregulation of macropinocytosis may be a common occurrence in forms of cell death labeled as necrosis, and it may therefore be more widespread than previously recognized.

Materials and Methods

Cell Culture

U251 glioblastoma cells were obtained from the DCT Tumor Repository (National Cancer Institute). Other cell lines were obtained from the same source or from the American Type Culture Collection. Cells were maintained at 37°C with 5% CO_2 in DMEM supplemented with 10% heat-inactivated fetal bovine serum. Phase-contrast images of the live cells were obtained by using an Olympus IX70 microscope equipped with a digital camera and SPOT imaging software (Diagnostic Instruments, Inc.).

[1] Unpublished data.

Table 1. Comparison of Methuosis with Other Common Forms of Cell Death

Characteristic*	Methuosis †	Autophagic	Paraptosis	Oncosis	Necroptosis	Necrosis	Apoptosis
Cytoplasmic vacuolation (origin)	+ (macropinosomes)	+ (autophagosomes, autolysosomes)	+ (ER, mitochondria)	+ (ER, mitochondria)	+ (ER, mitochondria)	+ (uncertain)	–
Cell swelling	+	–/+	+	+	+	+	–
Plasma membrane rupture	+	–	–	+	+	+	–
Membrane blebbing	–	–	–	+	–	–	+
Nucleosomal DNA fragmentation (laddering)	+	–/+(late)	–	–	–	–	+
Chromatin marginalization or condensation	–	–/+(late)	–	+	+	–	+
Caspase activation	+	–/+(late)	–	–	–	–/+	+
Mitochondrial membrane depolarization	?	–/+	+	+	+	+	+
ATP depletion	+	?	+	?	+	+	+
Lysosomal membrane permeabilization	–	?	–	+	?	+	–/+
Autophagic activity increased	+	+	?	?	+	+	–/+

Abbreviation: ER, endoplasmic reticulum.
*Information was compiled from the references cited in Discussion.
†Based on observations with U251 glioblastoma and other glioma cell lines listed in Supplementary Fig. S2. Morphologic features consistent with methuosis have also been observed when Ras(G12V) is expressed in MKN-1 and TMK-1 gastric carcinoma cells (15).

Generation of Stable Cell Lines for Inducible Expression of Active Ras and Rac

To generate stable cell lines capable of conditional Ras expression, U251 cells were nucleofected with pTet-on (Clontech), which encodes the reverse tet-responsive transcriptional activator. Cells were selected with 500 μg/mL G418 and clonal lines were tested in transient transfection assays to determine which ones gave the tightest Dox-regulated gene expression using the tet-responsive pTRE vector (Clontech). One such clone was used for generation of permanent cell lines by nucleofection with pTRE(*myc-H-RasG12V*) together with pTK-Hyg. Clones were selected in medium containing 200 μg/mL hygromycin + 200 μg/mL G418 and screened to measure the expression of myc-H-Ras(G12V) in response to 1 μg/mL Dox. The clonal line, U251-C18, was selected for use in the present studies, although other clones exhibited essentially identical morphologic phenotypes when Ras(G12V) expression was induced. For Rac1(G12V) expression, lentiviral particles containing the gene for myc-tagged Rac1(G12V) under the control of a tet-inducible promoter were generated by America Pharma Source, LLC. These were mixed with lentiviral particles containing a gene for blasticidin resistance and used to coinfect U251 pTet-on cells. Clones were selected in medium containing 10 μg/mL blasticidin and 200 μg/mL G418. Expression of myc-Rac1(G12V) was induced by adding 1 μg/mL Dox to the medium.

Retroviral Expression

Myc-tagged *H-Ras* constructs (*G12V* and *S17N*) were subcloned into the *Eco*R1-*Bam*H1 sites of the retroviral expression vector, pFBneo (Stratagene). Procedures for retrovirus production and infection of glioma cells have been described previously (22).

Nucleofection

H-Ras(G12V) was subcloned into pCMV5 that had been modified to encode an in-frame myc epitope tag (MEQKLISEEDL). The expression vector was introduced into U251 cells by nucleofection using the Nucleofector II system from Amaxa, Inc., with Solution T and program T-30. Other cell lines were nucleofected with different solutions and programs: HEK293 cells, Solution V with program Q-001; HeLa cells, Solution R with program I-013; and HEp2 cells, Solution V with program G-016.

Western Blot Analysis

Antibodies were obtained from the following sources: myc epitope, EMD Biosciences; PARP, BD PharMingen; laminA/C, Cell Signaling Technology; lactate dehydrogenase and α-tubulin, Sigma; and LC3 (APG8b, N-Term), Abgent. Protein was quantified in cell lysates by colorimetric assay using the Bio-Rad reagent (Bio-Rad, Inc.). SDS-PAGE and Western blot analyses were done as previously described (22) using enhanced chemiluminescent detection (GE Healthcare). Immunoblot signals were quantified using a Kodak 440CF image station or an Alpha Innotech FluorChem HD2 imaging system.

To block the lysosomal turnover of endogenous LC3-II, cells were incubated in medium containing protease inhibitors, E64D (10 μg/mL) and pepstatin A (10 μg/mL; Peptides International), for 48 h before Western blot analysis of LC3. Cells treated with 500 nmol/L staurosporine (Cayman Chemical Company) for 18 to 24 h served as positive controls for induction of PARP and lamin cleavage associated with apoptosis.

Cell Viability and Cell Cycle Distribution

The viability of individual cells was assessed by fluorescence microscopy using the Viability/Cytotoxicity Assay Kit (Biotium, Inc.), which measures hydrolysis of calcein acetoxy methylester (live) and uptake of ethidium homodimer III (dead). At least 50 cells per sample were counted to determine the percent dead population and all samples were analyzed in triplicate. The viability of cell populations in culture was quantified by metabolic activity assay, measuring the conversion of 3-(4,5-dimethylthiazol-2-yl)-2,5-diphenyltetrazolium bromide (MTT) to the formazan derivative using the Cell Growth Determination kit from Sigma. The formazan derivative

was quantified by measuring its absorbance at 570 nm with a Spectra Max 384 Plus plate reader. Caspase-3 activity was detected with the NucView fluorescence-based assay (Biotium) according to the directions supplied by the manufacturer.

To compare the relative levels of ATP in vacuolated versus nonvacuolated cells, the cells were collected by trypsinization and assayed using the CellTiter Glo kit from Promega. The luminescence produced by the ATP-dependent monooxygenation of luciferin by luciferase was normalized to the number of cells added to the assay, determined with a Coulter counter.

For colony-forming assays, cells were seeded in 100-mm dishes at 1,400 per dish. The day after plating, H-Ras(G12V) expression was induced in half of the cultures by inclusion of 1 μg/mL Dox in the medium. Medium was replaced in all cultures every 2 to 3 d. Colony formation was assessed after 3 wk by washing the cultures with PBS, fixing the cells for 10 min in ice-cold methanol, and staining for 10 min with 1% crystal violet in 35% methanol. Colonies containing at least 50 cells were counted under a dissecting microscope.

Cell cycle distribution was determined from DNA histograms generated by flow cytometric analysis of cells prepared as described (52) using a Beckman-Coulter EPIC XL MCL cytometer. Data were analyzed using Multicycle DNA cell cycle analysis software (Phoenix Flow Systems).

DNA fragments were isolated by the method of Herrmann et al. (53) and resolved by electrophoresis in a 1.2% agarose gel. Images were obtained using the FluorChem HD2 system after staining the gel with ethidium bromide.

Immunofluorescence Microscopy

Cells were prepared for immunofluorescence as previously described (27). Myc-tagged proteins were detected with a monoclonal antibody (EMD Biosciences) followed by goat anti-mouse IgG conjugated with Alexa Fluor 568 (Invitrogen). For detection of endogenous LC3, we used the purified rabbit polyclonal antibody APG8b (MAP1LC3B, N-Term) from Abgent, followed by goat anti-rabbit IgG conjugated with Alexa Fluor 488. Antibodies used for immunofluorescence localization of EEA1 and LAMP1, were obtained from Abcam and the Developmental Studies Hybridoma Bank, respectively. Cells were examined with a Nikon Eclipse 800 fluorescent microscope equipped with a digital camera and ImagePro software (Media Cybernetics) or with a Leica TCS SP5 multiphoton confocal microscope using 488- and 561-nm laser excitation lines.

Electron Microscopy

Cell pellets were fixed, dehydrated, and infiltrated as previously described (27). Ultrathin sections were collected on copper 300-mesh support grids, stained with uranyl acetate and lead citrate, and examined under a Philips CM 10 transmission electron microscope.

Uptake of Fluid-Phase and Organelle-Specific Tracers

Lucifer yellow and dextran-Alexa Fluor 488 (10,000 MW) were purchased from Invitrogen/Molecular Probes. Cells were incubated with Lucifer yellow (1.5 mg/mL in HBSS) for 15 min in a 37°C, 5% CO_2 incubator. Lucifer yellow was removed and the cells were washed once with HBSS. Phase-contrast and fluorescent images of the live cells were immediately taken using an Olympus IX70 microscope equipped with a digital camera and SPOT imaging software. Uptake of Lucifer yellow was quantified by flow cytometry. Briefly, cells were grown in phenol red–free medium, incubated with Lucifer yellow as described above, harvested by trypsinization, and suspended in HBSS. For each sample, 10,000 cells were analyzed with a Beckman-Coulter EPICS Elite ESP cytometer, with 488-nm excitation laser and 505- to 545-nm emission. The mean fluorescence intensity of the population was determined after subtraction of autofluorescence background obtained from parallel control samples incubated without Lucifer yellow. In some studies, the cells were preincubated with cytochalasin D (1 μmol/L; Sigma) for 30 min before the addition of Lucifer yellow.

For labeling with dextran-Alexa Fluor 488, the cells were washed twice with phenol red–free DMEM containing 10% fetal bovine serum, and then incubated with 0.5 mg/mL dextran-Alexa Fluor 488 in the same medium for the period of time indicated in the figure legends. The cells were washed twice in the same medium without the tracer, and then images of the live cells were acquired as described for Lucifer yellow staining. In some cases, cells were colabeled for 15 min with dextran-Af488 and human holotransferrin conjugated to Alexa Fluor 594 (Invitrogen/Molecular Probes) added at 5 μg/mL in serum-free DMEM.

Intracellular acidic compartments were labeled by incubating live cells at 37°C, with Lysotracker Red DND-99 (Invitrogen) added to phenol red–free DMEM at a final concentration of 1 μmol/L. Staining of intracellular compartments for cathepsin B activity was done by incubating live cells with Magic Red RR (Immunochemistry Technologies) according to the directions supplied by the manufacturer.

Disclosure of Potential Conflicts of Interest

No potential conflicts of interest were disclosed.

Acknowledgments

We thank Thomas Sawyer and Karen Domenico for help with flow cytometry, and William Gunning, Ph.D., and Michelle Lewandowski for assistance with electron microscopy.

References

1. Davis FG, Freels S, Grutsch J, Barlas S, Brem S. Survival rates in patients with primary malignant brain tumors stratified by patient age and tumor histological type: an analysis based on Surveillance, Epidemiology, and End Results (SEER) data, 1973-1991. J Neurosurg 1998;88:1–10.

2. McLendon RE, Halperin EC. Is the long-term survival of patients with intracranial glioblastoma multiforme overstated? Cancer 2003;98:1745–8.

3. Bredel M. Anticancer drug resistance in primary human brain tumors. Brain Res Brain Res Rev 2001;35:161–204.

4. Lefranc F, Brotchi J, Kiss R. Possible future issues in the treatment of glioblastomas: special emphasis on cell migration and the resistance of migrating glioblastoma cells to apoptosis. J Clin Oncol 2005;23:2411–22.

5. Lockshin RA, Zakeri Z. Apoptosis, autophagy, and more. Int J Biochem Cell Biol 2004;36:2405–19.

6. Zakeri Z, Bursch W, Tenniswood M, Lockshin RA. Cell death:programmed, apoptosis, necrosis or other? Cell Death Differ 1995;2:87–96.

7. Bursch W, Ellinger A, Gerner C, Frohwein U, Schulte-Hermann R. Programmed cell death (PCD). Apoptosis, autophagic PCD, or others? Ann N Y Acad Sci 2000;926:1–12.

8. Kanzawa T, Germano IM, Komata T, Ito H, Kondo Y, Kondo S. Role of

autophagy in temozolomide-induced cytotoxicity for malignant glioma cells. Cell Death Differ 2004;11:448–57.

9. Kanzawa T, Kondo Y, Ito H, Kondo S, Germano I. Induction of autophagic cell death in malignant glioma cells by arsenic trioxide. Cancer Res 2003;63:2103–8.

10. Yao KC, Komata T, Kondo Y, Kanzawa T, Kondo S, Germano IM. Molecular response of human glioblastoma multiforme cells to ionizing radiation: cell cycle arrest, modulation of the expression of cyclin-dependent kinase inhibitors, and autophagy. J Neurosurg 2003;98:378–84.

11. Takeuchi H, Kondo Y, Fujiwara K, Kanzawa T, Aoki H, Mills GB, Kondo S. Synergistic augmentation of rapamycin-induced autophagy in malignant glioma cells by phosphatidylinositol 3-kinase/protein kinase B inhibitors. Cancer Res 2005;65:3336–46.

12. Gozuacik D, Kimchi A. Autophagy as a cell death and tumor suppressor mechanism. Oncogene 2004;23:2891–906.

13. Levine B, Yuan J. Autophagy in cell death: an innocent convict? J Clin Invest 2005;115:2679–88.

14. Mathew R, Karantza-Wadsworth V, White E. Role of autophagy in cancer. Nat Rev Cancer 2007;7:961–7.

15. Chi S, Kitanaka C, Noguchi K, et al. Oncogenic Ras triggers cell suicide through the activation of a caspase-independent cell death program in human cancer cells. Oncogene 1999;18:2281–90.

16. Ishii N, Maier D, Merlo A, et al. Frequnt co-alterations of TP53, p16/CDKN2A, p14arf, PTEN tumor suppressor genes in human glioma cell lines. Brain Pathol 1999;9:469–79.

17. Kaul A, Overmeyer JH, Maltese WA. Activated Ras induces cytoplasmic vacuolation and non-apoptotic death in glioblastoma cells via novel effector pathways. Cell Signal 2007;19:1034–43.

18. Dunn WA, Jr. Studies on the mechanisms of autophagy: formationof the autophagic vacuole. J Cell Biol 1990;110:1923–33.

19. Kabeya Y, Mizushima N, Ueno T, et al. LC3, a mammalian homologue of yeast apg8p, is localized in autophagosome membranes after processing. EMBO J 2000;19:5720–8.

20. Tanida I, Minematsu-Ikeguchi N, Ueno T, Kominami E. Lysosomal turnover, but not a cellular level, of endogenous LC3 is a marker for autophagy. Autophagy 2005;1:84–91.

21. Ravikumar B, Vacher C, Berger Z, et al. Inhibition of mTOR induces autophagy and reduces toxicity of polyglutamine expansions in fly and mouse models of Huntington disease. Nat Genet 2004;36:585–95.

22. Zeng X, Overmeyer JH, Maltese WA. Functional specificity of the mammalian Beclin-Vps34 PI 3-kinase complex in macroautophagy versus endocytosis and lysosomal enzyme trafficking. J Cell Sci 2006;119:259–70.

23. Bar-Sagi D, Feramisco JR. Induction of membrane ruffling and fluid-phase pinocytosis in quiescent fibroblasts by ras proteins. Science 1986;233:1061–8.

24. Swanson JA, Watts C. Macropinocytosis. Trends Cell Biol 1995;5:424–8.

25. Schnatwinkel C, Christoforidis S, Lindsay MR, et al. The Rab5 effector Rabankyrin-5 regulates and coordinates different endocytic mechanisms. PLoS Biol 2004;2:1363–80.

26. Dunn WA, Jr. Studies on the mechanisms of autophagy: maturation of the autophagic vacuole. J Cell Biol 1990;110:1935–45.

27. Johnson EE, Overmeyer JH, Gunning WT, Maltese WA. Gene silencing reveals a specific function of hVps34 phosphatidylinositol 3-kinase in late versus early endosomes. J Cell Sci 2006;119:1219–32.

28. Futter CE, Collinson LM, Backer JM, Hopkins CR. Human VPS34 is required for internal vesicle formation within multivesicular endosomes. J Cell Biol 2001;155:1251–64.

29. Traganos F, Darzynkiewicz Z. Lysosomal proton pump activity: supravital cell staining with acridine orange differentiates leukocyte subpopulations. Methods Cell Biol 1994;41:185–94.

30. Paglin S, Hollister T, Delohery T, et al. A novel response of cancer cells to radiation involves autophagy and formation of acidic vesicles. Cancer Res 2001;61:439–44.

31. Cook NR, Row PE, Davidson HW. Lysosome associated membrane protein 1 (Lamp1) traffics directly from the TGN to early endosomes. Traffic 2004;5:685–99.

32. Czibener C, Sherer NM, Becker SM, et al. Ca^{2+} and synaptotagmin VII-dependent delivery of lysosomal membrane to nascent phagosomes. J Cell Biol 2006;174:997–1007.

33. Ridley AJ, Paterson HF, Johnston CL, Diekmann D, Hall A. The small GTP-binding protein rac regulates growth factor-induced membrane ruffling. Cell 1992;70:401–10.

34. Dharmawardhane S, Schurmann A, Sells MA, Chernoff J, Schmid SL, Bokoch GM. Regulation of macropinocytosis by p21-activated kinase-1. Mol Biol Cell 2000;11:3341–52.

35. Lambert JM, Lambert QT, Reuther GW, et al. Tiam1 mediates Ras activation of Rac by a PI(3)K-independent mechanism. Nat Cell Biol 2002;4:621–5.

36. Gobeil S, Boucher CC, Nadeau D, Poirier GG. Characterization of the necrotic cleavage of poly(ADP-ribose) polymerase (PARP-1): implication of lysosomal proteases. Cell Death Differ 2001;8:588–94.

37. Sperandio S, de BI, Bredesen DE. An alternative, nonapoptotic form of programmed cell death. Proc Natl Acad Sci U S A 2000;97:14376–81.

38. Wang Y, Li X, Wang L, et al. An alternative form of paraptosis-like cell death, triggered by TAJ/TROY and enhanced by PDCD5 overexpression. J Cell Sci 2004;117:1525–32.

39. Majno G, Joris I. Apoptosis, oncosis, and necrosis. An overview of cell death. Am J Pathol 1995;146:3–15.

40. Trump BF, Berezesky IK, Chang SH, Phelps PC. The pathways of cell death: oncosis, apoptosis, and necrosis. Toxicol Pathol 1997;25:82–8.

41. Suarez Y, Gonzalez L, Cuadrado A, Berciano M, Lafarga M, Munoz A. Kahalalide F, a new marine-derived compound, induces oncosis in human prostate and breast cancer cells. Mol Cancer Ther 2003;2:863–72.

42. Degterev A, Huang Z, Boyce M, et al. Chemical inhibitor of nonapoptotic cell death with therapeutic potential for ischemic brain injury. Nat Chem Biol 2005;1:112–9.

43. Han W, Li L, Qiu S, et al. Shikonin circumvents cancer drug resistance by induction of a necroptotic death. Mol Cancer Ther 2007;6:1641–9.

44. Kroemer G, Jaattela M. Lysosomes and autophagy in cell death control. Nat Rev Cancer 2005;5:886–97.

45. Syntichaki P, Tavernarakis N. Death by necrosis. Uncontrollable catastrophe, or is there order behind the chaos? EMBO Rep 2002;3:604–9.

46. Edinger AL, Thompson CB. Death by design: apoptosis, necrosis and autophagy. Curr Opin Cell Biol 2004;16:663–9.

47. Samara C, Syntichaki P, Tavernarakis N. Autophagy is required for necrotic cell death in *Caenorhabditis elegans*. Cell Death Differ 2008;15:105–12.

48. Hegde M, Roscoe J, Cala P, Gorin F. Amiloride kills malignant glioma cells independent of its inhibition of the sodium-hydrogen exchanger. J Pharmacol Exp Ther 2004;310:67–74.

49. Loo D, Pryer N, Young P, et al. The glycotope-specific RAV12 monoclonal antibody induces oncosis *in vitro* and has antitumor activity against gastrointestinal adenocarcinoma tumor xenografts *in vivo*. Mol Cancer Ther 2007;6:856–65.

50. Campbell SL, Khosravi-Far R, Rossman KL, Clark GJ, Der CJ. Increasing complexity of Ras signaling. Oncogene 1998;17:1395–413.

51. Cox AD, Der CJ. The dark side of Ras: regulation of apoptosis. Oncogene 2003;22:8999–9006.

52. Vindelov LL, Christensen IJ, Nissen NI. A detergent-trypsin method for the preparation of nuclei for flow cytometric DNA analysis. Cytometry 1983;3:323–7.

53. Herrmann M, Lorenz HM, Voll R, Grunke M, Woith W, Kalden JR. A rapid and simple method for the isolation of apoptotic DNA fragments. Nucleic Acids Res 1994;22:5506–7.